RSC Advances

ROYAL SOCIETY OF CHEMISTRY

www.rsc.org/advances

RSC Advances

PAPER

The optimal design of Co catalyst morphology on three-dimensional carbon sponge with low cost, inducing a better sodium borohydride electrooxidation activity

Received 00th January 20xx,
Accepted 00th January 20xx

DOI: 10.1039/x0xx00000x

www.rsc.org/

Ke Ye*, Xiaokun Ma, Xiaomei Huang, Dongming Zhang, Kui Cheng, Guiling Wang and Dianxue Cao*

The low-cost nano-flake Co@carbon sponge (Co NF@carbon sponge) electrode is prepared by a simple sponge carbonization method coupled with direct Co growth on the carbon sponge surface using the pulsed electrodeposition. The catalytic activity of sodium borohydride ($NaBH_4$) electrooxidation in alkaline medium are studied by cyclic voltammetry (CV) and chronoamperometry (CA). The Co NF@carbon sponge electrode reveals a unique three-dimensional (3D) nano-flake structure on the porous network skeleton with large specific surface area and exhibits superior catalytic performance. The oxidation current density of Co NF@carbon sponge electrode towards $NaBH_4$ achieves 248 mA cm^{-2} in 1 mol L^{-1} NaOH and 0.12 mol L^{-1} $NaBH_4$ solution at −0.55 V (vs. Ag/AgCl) accompanied with a considerable stability, which is remarkably higher than the electrocatalytic performance of $NaBH_4$ oxidation obtained previously with non-noble metals as catalysts. The induced high catalytic activity is greatly contributed to the excellent 3D nano-flake open structure and high electronic conductivity, which guarantees the full utilization of Co surfaces and allows the electrode to own higher electrocatalytic performance. The novel Co NF@carbon sponge electrode is a hopeful anode with low cost and high performance for the application of fuel cells that employ $NaBH_4$ as the fuel.

1. Introduction

Energy issued from traditional sources with limited reserves (e.g. fossil oil, coal and natural gas) is intrinsically inefficient and incurs serious environmental contamination. By contrast, fuel cells convert directly the chemical energy of a fuel to electrical power. They are attractive candidates for future power generators due to their high-energy conversion efficiency, silence, environmental affinity and good reliability[1–6]. As a clean and renewable energy resource, hydrogen generates power by electrochemical oxidation from fuel cells and its oxidation product is only water. However, the large problem of transportation and storage for H_2 discourages its commercial development. One feasible solution to solve this problem is employing direct borohydride fuel cells (DBFCs)[7–12]. Sodium borohydride ($NaBH_4$) was first used as an anodic fuel in 1962, indicating the advantages of high storage density and long-term stability in alkaline solution[13]. $NaBH_4$ oxidation is presently attractive interest as an alternative anode reaction for fuel cells because it displays numerous merits, such as a low thermodynamic potential (E^o = −1.24 V vs. SHE) which allows a high theoretical cell potential (1.64 V using O_2 as oxidant), high capacity (5.7 Ah g^{-1}), high energy density (9.3 Wh g^{-1} at 1.64 V), easy transportation, high hydrogen content (weight content of 10.6 %) and absence of CO poisoning[14–23].

The $NaBH_4$ can be directly adopted as a fuel for DBFCs, in which the complete electrooxidation of $NaBH_4$ generates theoretical maximum of eight electrons (Eq. (1))[24–26]:

$$BH_4^- + 8OH^- \rightarrow BO_2^- + 6H_2O + 8e^- \quad (1)$$

Otherwise, the $NaBH_4$ can be applied as the ''indirect fuel'' for fuel cells, actually as a hydrogen carrier[27,28]. In this case, heterogeneous hydrolysis of the BH_4^- generating gaseous hydrogen (Eq. (2)) is taken place in parallel with Eq. (1) on the metal-based catalysts[26,27,29,30]. After that, the as-formed hydrogen is electrooxidized at the anode part of fuel cells[28,30–33].

$$BH_4^- + 4H_2O \rightarrow B(OH)_4^- + 4H_2 \quad (2)$$

For the electrochemical oxidation of $NaBH_4$, the anodic electrocatalyst is one of the key components to optimize its catalytic performance. At present, the numerous investigation of electrocatalysts for $NaBH_4$ oxidation are mainly concentrated upon noble metals and their alloys including Pt[15,16,34], Pd[14,23], Au[1,16], Pt–Au[16,29], Pt–RE (rare earth)[35], Pt–Sn[20], Pt–Co[21], Au–Fe[18,22] and so on. However, the high cost and scarcity of precious metals significantly increase the total price of catalysts and largely restrict their developments. Hydrogen storage AB_5- and AB_2-type alloys are also studied as the electrocatalysts for DBFCs anode, but the catalytic activity of these alloys is unsatisfactory for the practical applications of fuel cells[36–40]. As a low-cost metal, transition metals such as Ni[19,24–26], Co[21,22,27,31–33], Cu[19,22,41] and Fe[18,22], which are much

Key Laboratory of Superlight Materials and Surface Technology of Ministry of Education, College of Materials Science and Chemical Engineering, Harbin Engineering University, Harbin, 150001, P.R. China. E-mail addresses: yeke@hrbeu.edu.cn (K. Ye); caodianxue@hrbeu.edu.cn (D. Cao)

cheaper than platinum and palladium, are good candidates to catalyze anodic reactions of $NaBH_4$ in DBFCs. Among the transition metals, cobalt is identified as a promising electrocatalyst for $NaBH_4$ oxidation, ascribing to its high ability for breaking the B–H bonds in BH_4^- [27,28,31]. However, the catalytic property of current Co catalyst was not so high for $NaBH_4$ electrooxidation. In consequence, the improvement of electrocatalytic performance of Co material is urgent and significant for exploiting the low-cost and high-activity DBFCs. One of the most effective solutions to enhance the electrochemical performance of catalysts is controlling the electrocatalysts size in nanometer and fabricating the electrocatalysts with three-dimensional (3D) structures[42–47]. X. Wang et al.[23] reported that Pd nanospheres supported on carbon with the average Pd crystallite size of 3.8 nm exhibited a high electrocatalytic activity for BH_4^- oxidation. The DBFCs using these nano-sized Pd electrocatalysts showed as high as 48.4 mW cm^{-2} power densities at a discharge current density of 54.8 mA cm^{-2}. D. Duan and co-workers[25] prepared the nano-sized Ni@Au catalysts on carbon with the average size of ~ 10 nm and they also proved that the electrocatalysts displayed excellent catalytic activity towards the BH_4^- oxidation. Thus, the aim of this work is to achieve the nano-sized electrocatalysts with a 3D open structure for improving the electrooxidation activity of $NaBH_4$. In addition, an outstanding current-collecting substrate is also one of the decisive factors that determine the catalytic activity of an electrode. Carbon materials (e.g. carbon fiber cloth, carbon paper) are extensively applied as the current collectors, because of their high electronic conductivity[20–22,48,49]. Nonetheless, their flat structures relatively decrease the surface utilization of electrocatalysts, leading to the poor catalytic activity of electrodes. 3D porous structures are one of the optimum candidates for carbon substrate by reason of their excellent porosity and large surface area, which make the electrolyte ions simply permeate into the whole matrix surface and increase the utilization of catalyst surfaces[50,51]. Sponge (polyurethane foam), possessing a 3D open network structure, is very cheap and popular in our daily lives (e.g. used in the sofa, seat cushion, backrest, and so on)[50,51]. Under general conditions, the outdated products containing sponge will be easily discarded as the rubbish, which causes the serious environmental pollution. For this reason, the waste sponge should be essentially recycled.

In this work, the carbon sponge with superiorly porous 3D structures and inexpensive price was facilely prepared by the high-temperature carbonization of sponge. The as-obtained carbon sponge substrate owned splendid electronic conductivity and first-class stability in the alkaline medium. Then, the cobalt electrocatalysts with different morphologies (nanoparticles, nanoflakes and porosities) were directly deposited on the carbon sponge surface using the pulsed potential electrodeposition without any binder. The composite Co@carbon sponge electrodes had a unique 3D structure, which provided more electrochemical active sites and assured easy access of reactants to the catalyst surfaces. The catalytic activity of $NaBH_4$ electrooxidation on the Co@carbon sponge electrodes was systematically examined in alkaline solutions. The nano-flake Co@carbon sponge materials demonstrated the highest catalytic performance, stability and tolerance towards $NaBH_4$ electrooxidation among the three electrodes in NaOH solution, revealing a promising application in the fuel cells using $NaBH_4$ as anodic fuel.

2. Experimental

2.1. Preparation of Co@carbon sponge electrodes

Fig. 1 shows the schematic diagram of the synthesis for the Co@carbon sponge electrodes. The carbon sponge substrate was facilely fabricated by the high-temperature carbonization. A piece of sponge (polyurethane foam, 10 mm × 10 mm × 1 mm) was rinsed in acetone and ethanol sequentially by ultrasonic methods. After cleaning with the deionized water several times and blow-drying under flowing nitrogen (99.999%) gas, the sponge was first immersed in a 30 mL polyamide acid (PAA) solution with adding 15 mL N,N-dimethylacetamide (DMAC) for 1 h. The PAA and DMAC molecules in the free space between the porous structures of sponge would be easily adsorbed onto the sponge surface of microscopic skeleton. Afterwards, the composite sponge was removed from the solution and dried at 60 °C in a vacuum oven for 10 h. Then, the dried composite sponge was further annealed under nitrogen (99.999%) atmosphere with a flow rate of 40 mL min^{-1} at 900 °C in a tube furnace (SK-12, Longjiang) to form the carbon sponge electrode. The duration of carbonization reaction was 1 h, followed by cooling the samples to room temperature under nitrogen gas.

The Co NP@carbon sponge, Co NF@carbon sponge and Co PR@carbon sponge electrodes were prepared by the pulsed electrodeposition of nano-particulate, nano-flake and porous Co directly on the three-dimensional carbon sponge in the 0.2 mol L^{-1} $CoCl_2$ + 0.5 mol L^{-1} H_3BO_3 + 0.4 mol L^{-1} NH_4Cl + 1.0 mol L^{-1} KCl solutions (Fig. 1). The electrochemical deposition was conducted in a three-electrode system controlled by potentiostatic instrument (Autolab PGSTAT302, Eco Chemie). A piece of carbon sponge substrate and a platinum foil (10 × 10 mm) were served as the working electrode and counter electrode, respectively. A saturated Ag/AgCl electrode was employed as the reference electrode, and all potentials were referred to the Ag/AgCl electrode. The nano-particulate, nano-flake and porous Co were controllably achieved by the pulsed potential electrodeposition method (Fig. 1). The deposition frequency was 2.5 Hz. The lower potential limit (E_l) was fixed at −1.0 V, and the upper potential limit (E_u) was changed to be −0.1, −0.2 and −0.3 V, respectively. The electrodeposition time was ~ 30 min and the loading of Co catalysts on the obtained Co NP, Co NF and Co PR@carbon sponge electrodes was controlled to be the same at 7 mg cm^{-2}. The Co loading was checked by using an inductive coupled plasma emission spectrometer (ICP, Xseries II, Thermo Scientific). All the chemicals were analytical grade and used without further purification. Ultra-pure water (Millipore, 18 MΩ cm) was applied in this whole work.

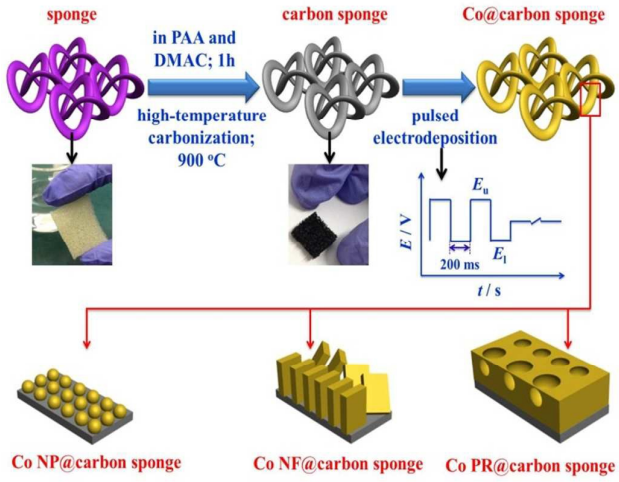

Fig. 1 Schematic depiction of the fabrication process of Co@carbon sponge electrodes.

2.2. Characterizations and electrochemical measurements of the deposited Co on the carbon sponge electrodes

The surface morphology of the deposited Co catalysts on the carbon sponge substrate was examined using a scanning electron microscope (SEM, JEOL JSM-6480) and transmission electron microscope (TEM, FEI Teccai G2S-Twin, Philips). The structure of the electrodes was characterized by an X-ray diffractometer (XRD, Rigaku TTR III) equipped with Cu-Kα radiation (λ = 0.1514178 nm) at a scan rate of 5° min^{-1}. The Co electrocatalysts that used for the TEM examination were obtained as the following steps: first of all, the deposited Co films were peeled off from the Co@carbon sponge electrodes by ultrasonic method and scattered in a 10 mL ethanol solution. Then, the obtained suspension was dropped onto the lacey support film.

The catalytic activity of the obtained Co@carbon sponge electrodes for $NaBH_4$ electrooxidation was measured by cyclic voltammetry (CV) and chronoamperometry (CA) in a standard three-electrode system with saturated Ag/AgCl reference electrode and Pt counter electrode. The electrolyte for $NaBH_4$ electrooxidation was $NaBH_4$-containing NaOH aqueous solution. The temperature of electrolyte was precisely adjusted by electric heating thermostatic water bath (±1 °C). All measurements not mentioned temperatures were tested at ambient temperature (20 °C). The current densities reported in this work were calculated by the geometrical area of electrodes (1 cm^2).

3. Results and discussion

3.1. Characterization of the Co@carbon sponge electrodes

The Co@carbon sponge electrodes were obtained by the pulsed electrochemical deposition of Co catalysts with different surface morphologies on the three-dimensional (3D) carbon sponge under different upper potential limit (E_u). Fig. 2 presents the low-magnification and high-magnification SEM images of Co NP@carbon sponge, Co NF@carbon sponge and Co PR@carbon sponge electrodes prepared at E_u of −0.1, −0.2 and −0.3 V, respectively. The naked carbon sponge substrate was also shown in Fig. 2a and b for comparison. Carbon sponge as the current collector fabricated by the high-temperature carbonization can acquire many merits containing such as high electronic conductivity and desirable stability in the rigorous alkaline medium. It is obvious from Fig. 2a that the carbon sponge was composed of many porous network cells with the length of ~ 300 μm and the width of ~ 150 μm. The SEM image (Fig. 2b) with a high magnification apparently indicated that the surface of carbon sponge electrode was lumpy and rugged. These superiorly open web-like structures can supply a three-dimensional porous framework for the cobalt electrodeposition. In addition, the carbon sponge owns outstanding electronic conductivity and good stability, which made it a favorable support and current collector for cobalt electrocatalysts. Fig. 2c and d show the SEM images of typical Co NP@carbon sponge electrode with different magnification, indicating that many cobalt nanoparticles equably formed on the 3D skeleton surface of carbon sponge after the electrodeposition of Co. It can be seen from Fig. 2e that the dense Co catalysts were uniformly deposited on the carbon sponge surface in a low-magnification SEM image. The higher magnification SEM image (Fig. 2f) of Co NF@carbon sponge clearly displayed that the Co layer composed of numerous Co nanoflakes intercrossing with each other. Some Co nanoflakes with ultrathin thickness grew perpendicularly from the matrix and demonstrated a 3D open nanostructure, which allowed electrolytes to contact the full electrode surface. In addition, the formed Co surface revealed a rough and irregular appearance, which was comprised by sheet-like structures with uneven profiles on account of the ultrathin characters. A 3D loose nano-flake structure with plenty of open space was established on the Co NF@carbon sponge electrode, which would be very suitable for the mass transport of electrolyte ions during the electrochemical reaction process and might result in an excellent electrocatalytic performance. As can be observed from Fig. 2g, the Co film including some holes was evenly distributed on the backbone surface of carbon sponge. The porous structure of Co film can be seen more distinctly in the amplifying SEM image (shown in Fig. 2h). These results manifest that the surface morphologies of Co catalysts transforms from nanoparticles formed at E_u of −0.1 V to nanoflakes prepared at E_u of −0.2 V and eventually to porous morphology obtained at E_u of −0.3 V with the decrease of E_u. As a consequence, the morphologies of Co catalysts can be facilely controlled by altering the upper potential limit using the pulsed potential electrodeposition method. More importantly, the as-prepared Co NP@carbon sponge, Co NF@carbon sponge and Co PR@carbon sponge electrodes may be especially appropriate to $NaBH_4$ electrooxidation in alkaline medium. These unique structures make the electroactive Co own a large specific surface area and ensure the full utilization of Co catalysts.

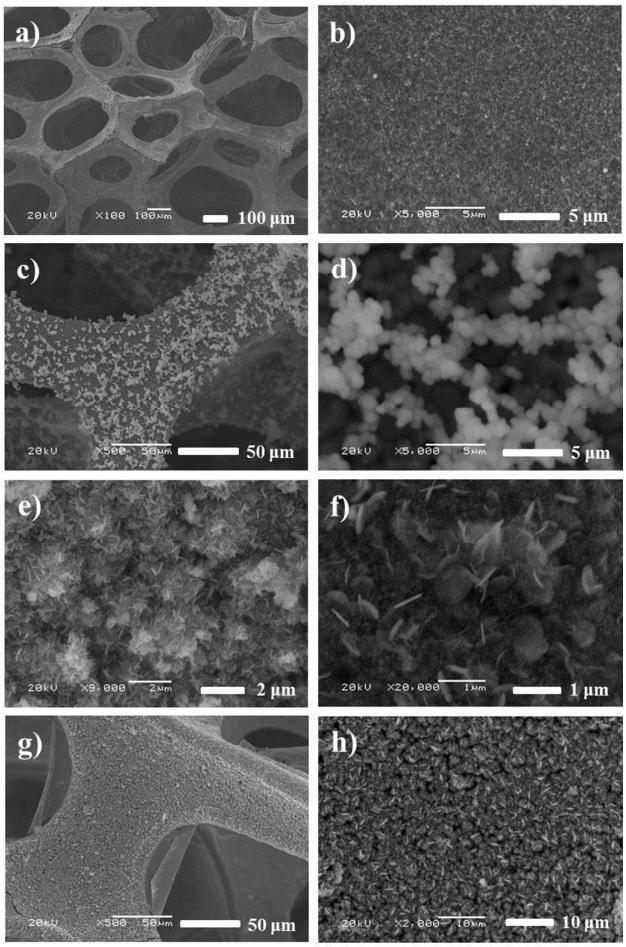

Fig. 2 Different-magnification SEM images of the carbon sponge substrate (a and b); nano-particulate Co@carbon sponge (Co NP@carbon sponge) electrode (c and d); nano-flake Co@carbon sponge (Co NF@carbon sponge) electrode (e and f); porous Co@carbon sponge (Co PR@carbon sponge) electrode (g and h).

In order to further determine the detailed morphologies of Co film, transmission electron microscopy measurement was carried out. Fig. 3 exhibits the TEM images of Co electrocatalysts prepared at the different upper potential by pulsed potential electrodeposition. The TEM image of the Co formed at E_u of −0.1 V was shown in Fig. 3a and revealed that the appearance of Co film was nanoparticles with different sizes. The diameter ranges of the nanoparticles were from ~100 nm to ~300 nm. It can be seen from Fig. 3b that the Co fabricated at E_u of −0.2 V was consisted of many different-sized superthin nanoflakes. The shape of the Co nanoflakes was seemed to be hexagon. The side length of the small-sized hexagon nanoflakes was ~75 nm and that of the large-sized hexagon was ~150 nm. The individual Co nanoflake with the average side length of ~ 100 nm was exhibited in Fig. 3c. Some parts of the hexagon was shattered and missing in the red frame (Fig. 3c), which was caused by the ultrasonic exfoliation in the preparation process of TEM samples. Obviously, the surfaces and margins of the Co nanoflake are fantastically rough, which will markedly enlarge the specific surface area of the Co NF@carbon sponge electrode. Moreover, hydrogen gas generated by $NaBH_4$ hydrolysis can fast move away from the Co electrocatalysts, avoiding the surface active sites of Co hindered by the adsorbed gas bubbles. The acquired Co NF@carbon sponge electrode with a novel 3D nano-flake structure may be especially fit for $NaBH_4$ electrooxidation in alkali. Fig. 3d demonstrates the TEM images of Co film produced at E_u of −0.3 V. Combining with the results of SEM image observed in Fig. 2h, it can be concluded that the porous microstructures of Co film were composed of some anomalous sheets with micron sizes.

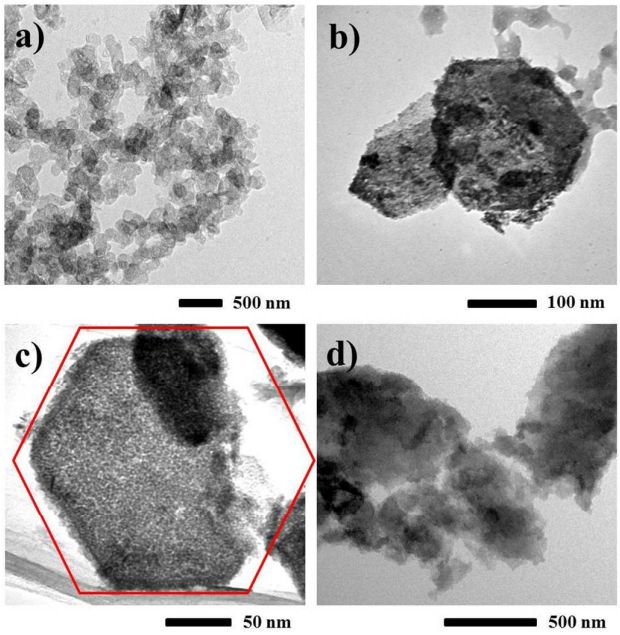

Fig. 3 TEM image of the Co NP@carbon sponge electrode (a); low-magnification and high-magnification TEM images of the Co NF@carbon sponge electrode (b and c); TEM image of the Co PR@carbon sponge electrode (d).

The XRD patterns of carbon sponge substrate, Co NP@carbon sponge, Co NF@carbon sponge and Co PR@carbon sponge electrodes were shown in Fig. 4. It was obvious that two broad diffraction peaks of the carbon sponge substrate centered at 25° and 44°, which can be identified as representative carbon peaks to confirm the existence of carbon[52]. By comparison with the carbon sponge, three sharp diffraction peaks of the Co NP@carbon sponge electrode locating at 44°, 52° and 76° matched well with the (111), (200) and (220) planes of cobalt metal, respectively, according to the standard crystallographic spectrum of Co (JCPDS card No. 15-0806). It displayed that Co emerged in the metallic state by the pulsed electrodeposition. XRD patterns of the Co NF@carbon sponge and Co PR@carbon sponge electrodes also demonstrated the typical traits of metallic cobalt. Differing from the Co NP@carbon sponge, the intensities of the Co diffraction peaks on the Co NF@carbon sponge and Co PR@carbon sponge electrodes

were higher than that on the Co NP@carbon sponge electrode. The peaks of Co NF@carbon sponge electrode showed the highest intensity, indicating that the Co nanoflakes contained the best well-crystallized cobalt crystals among the three catalytic electrodes. Besides, the main peak intensities of carbon sponge were significantly decreased after the deposition of Co catalysts, exhibiting that nano-particulate, nano-flake and porous Co were completely and homogeneously coated on the surface of carbon sponge.

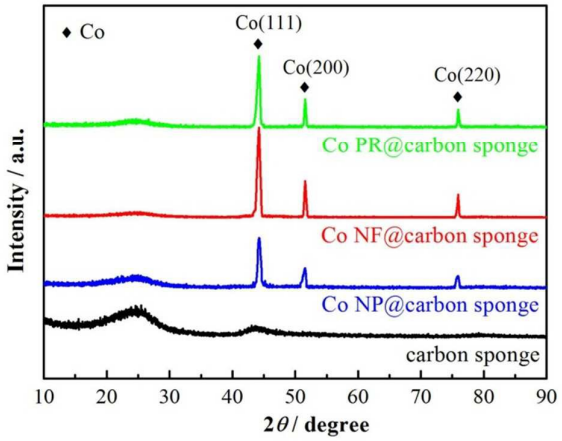

Fig. 4 XRD patterns of the carbon sponge substrate, Co NP@carbon sponge, Co NF@carbon sponge and Co PR@carbon sponge electrodes.

3.2. Catalytic performance of Co@carbon sponge electrodes for $NaBH_4$ electrooxidation

Fig. 5a shows the typical cyclic voltammograms (CVs) of the carbon sponge substrate, Co NP@carbon sponge, Co NF@carbon sponge and Co PR@carbon sponge electrodes tested in 1 mol L^{-1} NaOH solution. Apparently, there was no distinct redox peaks observed on the carbon sponge, suggesting that carbon sponge was steady in alkaline media. In contrast, a couple of oxidation/reduction peaks was readily appeared at −0.76 V/−1.05 V on the Co NP@carbon sponge electrode, exhibiting the typical characteristics of metallic Co in alkali, which was attributed to the inter-conversion of $Co/Co(OH)_2$[31,32,53]. The CVs of Co NF@carbon sponge and Co PR@carbon sponge electrodes revealed the similar response, whereas the $Co/Co(OH)_2$ current response on the Co NF@carbon sponge was more evidently viewed than that on the Co NP and Co PR@carbon sponge in the measured potential window. It hints that nano-flake Co owns greater catalytic property than nano-particulate Co and porous Co electrocatalysts.

For the sake of further verify that the Co NF@carbon sponge electrode was the optimum catalyst, the comparative CVs for $NaBH_4$ electrooxidation in 1 mol L^{-1} NaOH solution containing 0.12 mol L^{-1} $NaBH_4$ at the different electrodes were investigated in Fig. 5b. As seen, the carbon sponge substrate showed no electrocatalytic performance for $NaBH_4$ oxidation and no distinct redox peaks appeared on the carbon sponge. On the contrary, there were obvious current responses on the Co NP@carbon sponge electrode. The two oxidation peaks of Co NP@carbon sponge electrode located at −0.71 V and −0.52 V was corresponded to the electrooxidation reaction of hydrogen (Eq. (3)) and $NaBH_4$ (Eq. (1)), respectively[13,27,31,32]. Hydrogen gas was generated by the hydrolysis reaction of $NaBH_4$ (Eq. (2))[13,16–19,27]. The similar phenomena can also be discovered on the Co PR and Co NF@carbon sponge electrodes and the current densities at the same potential improved relatively in the order of Co NP, Co PR and Co NF@carbon sponge, showing that the Co NF@carbon sponge electrode had the highest catalytic activity towards $NaBH_4$ oxidation among the three electrodes. The current density value of Co NF@carbon sponge reached 257 mA cm^{-2} at the potential of −0.52 V, which was 2 times of Co PR@carbon sponge (127 mA cm^{-2}) and 3 times of Co NP@carbon sponge (86 mA cm^{-2}), respectively. The high electrocatalytic property of Co NF@carbon sponge electrode may be attributed to its large specific surface area, which was most likely offered by the unique 3D nano-flake structure and outstanding open network skeleton of carbon sponge.

$$H_2 + 2OH^- \rightarrow 2H_2O + 2e^- \quad (3)$$

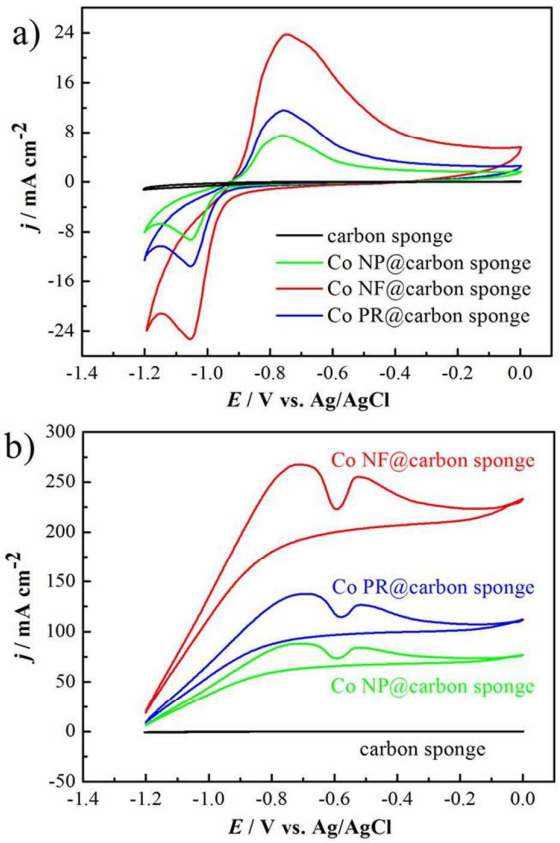

Fig. 5 Cyclic voltammograms of the carbon sponge substrate, Co NP@carbon sponge, Co NF@carbon sponge and Co PR@carbon sponge electrodes in 1 mol L^{-1} NaOH solution at a scan rate of 10 mV s^{-1} (a); comparative cyclic voltammograms of the carbon sponge substrate, Co NP@carbon sponge, Co NF@carbon sponge and Co PR@carbon sponge electrodes in 1 mol L^{-1} NaOH and 0.12 mol L^{-1} $NaBH_4$ at a scan rate of 10 mV s^{-1} (b).

The effects of $NaBH_4$ concentration on the electrocatalytic performance of the Co NF@carbon sponge electrode for $NaBH_4$ electrooxidation were inspected in Fig. 6. The $NaBH_4$ concentration was varied from 0.03 to 0.12 mol L^{-1} (Fig. 6a) at low concentration and from 0.12 to 0.50 mol L^{-1} (Fig. 6b) at high concentration in 1 mol L^{-1} NaOH solution, respectively. It was clear that the enhancement of $NaBH_4$ concentration resulted in a marked increase for the anodic current densities, displaying a powerful electrocatalytic property of the Co NF@carbon sponge electrode towards $NaBH_4$ oxidation. At low $NaBH_4$ concentrations, the anodic peaks of both hydrogen and $NaBH_4$ appeared distinctly in Fig. 6a. The current densities of $NaBH_4$ electrooxidation achieved 107 mA cm^{-2} at the peak potential of −0.72 V in the 0.03 mol L^{-1} $NaBH_4$ solutions, and increased to 257 mA cm^{-2} at the peak potential of −0.52 V with increasing the $NaBH_4$ concentration to 0.12 mol L^{-1}.

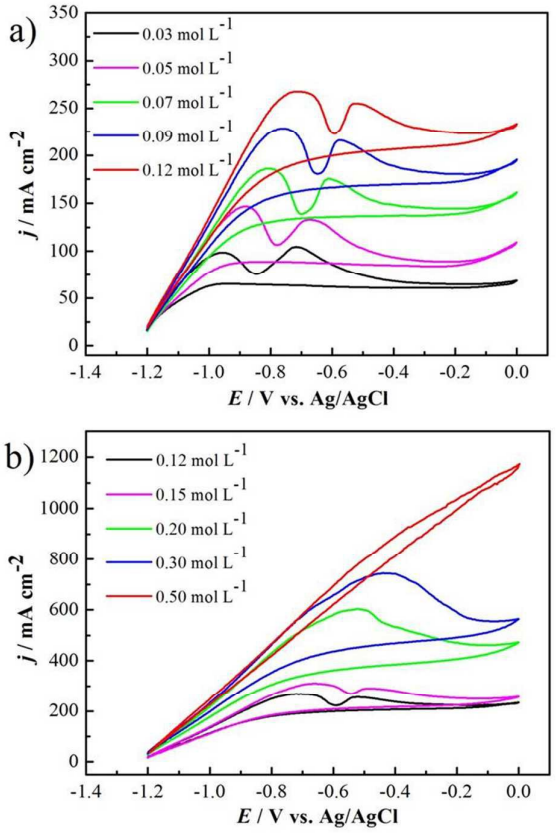

Fig. 6 Cyclic voltammograms of the Co NF@carbon sponge electrode in 1 mol L^{-1} NaOH with adding the low concentration of x mol L^{-1} $NaBH_4$ (x = 0.03, 0.05, 0.07, 0.09 and 0.12) (a); with adding the high concentration of x mol L^{-1} $NaBH_4$ (x = 0.12, 0.15, 0.20, 0.30 and 0.50) at a scan rate of 10 mV s^{-1} (b).

Likewise, the oxidation current densities of hydrogen also boosted with increasing the $NaBH_4$ concentration from 0.03 to 0.12 mol L^{-1}. In addition, the anodic peak potentials of both hydrogen and $NaBH_4$ moved positively with the increase of $NaBH_4$ concentration from 0.03 to 0.12 mol L^{-1}. Fig. 6b showed that the oxidation current densities of both hydrogen and $NaBH_4$ continued to increase with further increasing the $NaBH_4$ concentration to a high level. Besides, the oxidation peak potentials of both hydrogen and $NaBH_4$ continuously shifted in the positive direction and merged to be one broad peak as the $NaBH_4$ concentration attaining to 0.20 mol L^{-1}, and finally disappeared at high $NaBH_4$ concentration of 0.50 mol L^{-1}.

Table 1 Comparison of the catalytic performance (mA cm^{-2} mg^{-1}) for $NaBH_4$ electrooxidation on the different non-precious electrodes at −0.55 V (vs. Ag/AgCl)

Electrode	BH_4^- concentration (mol L^{-1})	Performance (mA cm^{-2} mg^{-1})	Ref.
AB_5-type alloy	0.1	0.1	36
AB_5-type alloy/Si	1.0	0.4	37
$LaNi_{4.5}Al_{0.5}$-Au	1.0	0.7	38
AB_5-type alloy/Ti-Zr	1.0	1.3	39
AB_5/MWNTs	0.1	1.9	40
Co/MWNTs/CC	0.1	17.5	31
Co/graphite/paper	0.1	18.0	32
Co/MWNTs/plastic	0.1	19.2	33
Ni/MWNTs	0.1	23.5	54
Co NF@carbon sponge	0.12	35.4	This work

(mg means the loading of catalysts, mg $(catalyst)^{-1}$)

Fig. 7a exhibits the influence of NaOH concentration for $NaBH_4$ electrooxidation on the Co NF@carbon sponge electrode. The NaOH concentrations were varied with fixing the $NaBH_4$ concentration at 0.12 mol L^{-1}. It is evident that the oxidation current densities of $NaBH_4$ peaks significantly decreased from 257 mA cm^{-2} to 145 mA cm^{-2} with increasing the NaOH concentration from 1 to 3 mol L^{-1}, revealing that excessive electrolyte made no contribution to improve the activity of $NaBH_4$ electrooxidation. In general, the fuel ($NaBH_4$) reacts with supporting electrolyte (NaOH) in a definite ratio. On the basis of Eq. (1), the appropriate proportion of $[BH_4^-]/[OH^-]$ is 0.125. The proportional numerical value of $[BH_4^-]/[OH^-]$ dropped much less than 0.125 after increasing the NaOH concentration higher than 2 mol L^{-1}, suggesting that the amount of fuel ($NaBH_4$) was completely insufficient. Since BH_4^- and OH^- reactant ions diffused simultaneously to the surface of Co NF@carbon sponge electrode during the $NaBH_4$ oxidation reaction, the current density of $NaBH_4$ electrooxidation decreased with inadaptable proportion of fuel/supporting electrolyte. Furthermore, the oxidation peak potentials of $NaBH_4$ changed relatively to the negative direction with the increase of NaOH concentration, which can be explained by Nernst formula. As expressed in Eq. (1), the reversible electrode potential reduced with the enhancement of $[OH^-]$. The on-going addition of NaOH as the reactant unquestionably facilitated the reaction of Eq. (1) at more negative potentials. Moreover, the more serious hydrolysis effect of $NaBH_4$ was appeared and caused by superfluous NaOH, resulting in the profiles of CVs (Fig. 7a) became noisier with increasing the NaOH concentration. Most important of all, the oxidation current density of $NaBH_4$ on the Co NF@carbon sponge achieved 248 mA cm^{-2} and 35.4 mA cm^{-2} mg^{-1} (mg

means the loading of catalysts, mg $(Co)^{-1}$) in 0.12 mol L^{-1} $NaBH_4$ and 1 mol L^{-1} NaOH solutions at −0.55 V, which was much higher than the previous literatures[36–40,31–33,54], certifying that the low-cost Co NF@carbon sponge electrode had remarkably higher electrocatalytic performance to $NaBH_4$ electrooxidation. The comparable catalytic activities of the Co, Ni, AB_5-type hydrogen storage alloys and Co NF@carbon sponge electrodes were demonstrated in Table 1. The high catalytic property of Co NF@carbon sponge electrode for $NaBH_4$ electrooxidation may be owing to the highly porous 3D skeleton of carbon sponge and especially its open nanoflake structure, benefitting for the faster diffusion of fuel during the catalytic reaction and enabling the full utilization of Co surfaces and thereby making the electrode have higher electrochemical activity.

The electrochemical stability of Co NF@carbon sponge electrode at different polarization potentials was studied by chronoamperometric test. Fig. 7b demonstrates the chronoamperometric curves (CAs) recorded in 0.12 mol L^{-1} $NaBH_4$ and 1 mol L^{-1} NaOH solutions at different potentials. The oxidation current densities at all the applied potentials (−0.5, −0.6, −0.9 and −1.0 V) became stable almost without any reduction after a primal decay, indicating that the Co NF@carbon sponge electrode maintained a steady state during the electrocatalytic process of hydrogen and $NaBH_4$ electrooxidation. Besides, the oxidation current densities promoted with altering the potential value to be more positive, which was in good accordance with the CV results represented in Fig. 7a. So the Co NF@carbon sponge electrode owns excellent electrocatalytic stability and may be a highly hopeful anode for the application of direct $NaBH_4$ fuel cells.

The influence of reaction temperature on the catalytic activity of $NaBH_4$ electrooxidation on the Co NF@carbon sponge electrode was further examined in Fig. 8. The CAs of $NaBH_4$ electrooxidation measured at different temperatures were shown in Fig. 8a. The catalytic performance of $NaBH_4$ electrooxidation was accelerated notably by rising the temperature. The oxidation current densities at −0.55 V improved from 165 to 282 mA cm^{-2} with raising the reaction temperature from 283.15 to 323.15 K, which proves that the higher temperature often brings about the quicker electrode reaction dynamics. However, the high-temperature CAs (313.15 K and 323.15 K) showed a slight attenuation, which

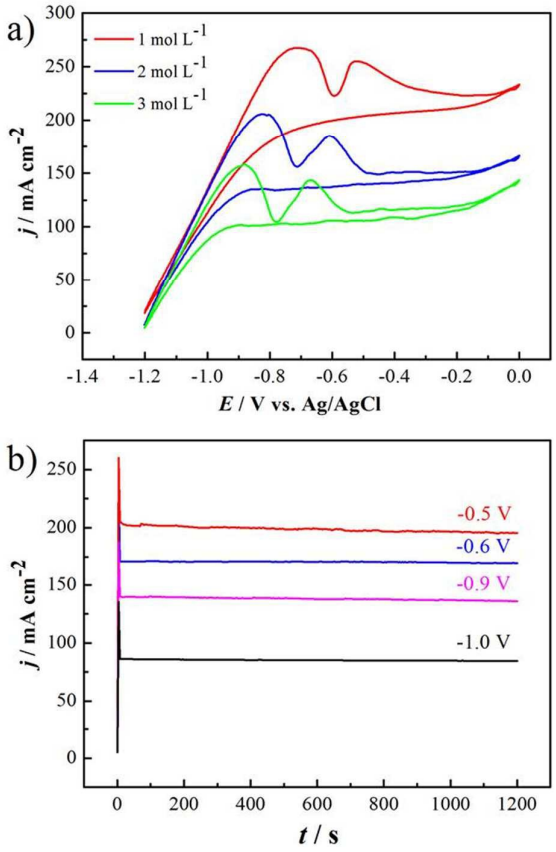

Fig. 7 Cyclic voltammograms of the Co NF@carbon sponge electrode in 0.12 mol L^{-1} $NaBH_4$ and x mol L^{-1} NaOH (x = 1, 2 and 3) at a scan rate of 10 mV s^{-1} (a); chronoamperometric curves for $NaBH_4$ electrooxidation on the Co NF@carbon sponge electrode at different applied potentials in 1 mol L^{-1} NaOH and 0.12 mol L^{-1} $NaBH_4$ (b).

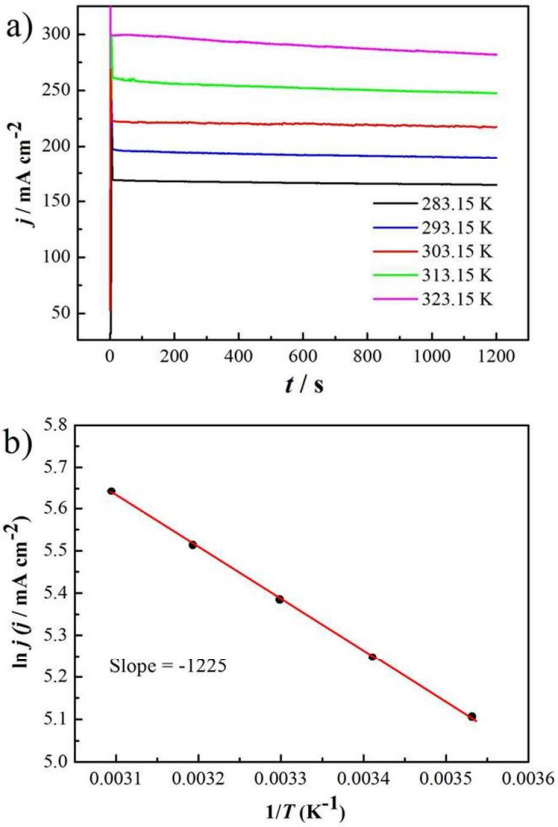

Fig. 8 Chronoamperometric curves of the Co NF@carbon sponge electrode in 1 mol L^{-1} NaOH and 0.12 mol L^{-1} $NaBH_4$ at −0.55 V with different temperatures (a); Arrhenius plot of the current densities for $NaBH_4$ electrooxidation on the Co NF@carbon sponge electrode (b).

may be due to the persistent consumption of fuel ($NaBH_4$) during the testing process at high temperatures. Additionally, the CAs at high temperatures (313.15 K and 323.15 K) got much noisier than those at low temperatures (283.15 K, 293.15 K and 303.15 K). The high temperature will boost the hydrolysis rate of $NaBH_4$ and generate more hydrogen gas[30–33]. The hydrogen moves away from the surface of Co NF@carbon sponge electrode and perturb the stability of electrolyte solution. Fig. 8b displays the Arrhenius plot of the current densities at −0.55 V for $NaBH_4$ electrooxidation. The logarithm of current densities (ln *j*) was plotted against the reciprocal of absolute temperature ($1/T$). Based on the Arrhenius equation (Eq. 4)[2,31], the activation energy of $NaBH_4$ electrooxidation was calculated to be 10.18 kJ mol^{-1} from the slope of ln *j* versus $1/T$, which was lower than that of the N_2H_4 electrooxidation on Co/carbon fiber cloth, the H_2O_2 electrooxidation on nickel nanowire arrays and the $NaBH_4$ electrooxidation on Co/MWNTs/CC electrode[2,31,55]. As a consequence, $NaBH_4$ is a prospective fuel with fast oxidation kinetics enabling the application of inexpensive Co NF@carbon sponge catalysts.

$$\frac{\partial \ln j}{\partial T} = -\frac{E_a}{RT^2} \quad (4)$$

where *j* is the current density (mA cm^{-2}), *T* is the thermodynamic temperature (K), *R* is the molar gas constant (8.314 J mol^{-1} K^{-1}), and E_a is the activation energy (J mol^{-1}).

4. Conclusions

In summary, novel Co@carbon sponge electrodes were successfully fabricated via a facile and green sponge carbonization method followed by direct Co electrodeposition using the pulsed potential electrodeposition without any template, seed and surfactant. Highly conductive carbon sponge was simply obtained as the basic support for metallic Co directly grown on its surface, forming unique three-dimensional structures. The surface morphology and the electrocatalytic activity of the deposited Co for the $NaBH_4$ oxidation were strongly dependent on the upper potential limit (E_u) of the pulsed electrodeposition. With the decrease of E_u, the surface morphology of Co catalysts changes from nanoparticles formed at E_u of −0.1 V to nanoflakes prepared at E_u of −0.2 V and eventually to porous morphology obtained at E_u of −0.3 V. Furthermore, the surface morphology of Co catalysts on the carbon sponge plays an important role in determining the electrocatalytic performance of $NaBH_4$ oxidation. The Co NF@carbon sponge electrode possesses much higher activity than Co NP@carbon sponge and Co PR@carbon sponge electrodes. The Co NF@carbon sponge electrode composing of unique intercrossed Co nanoflakes on the carbon sponge with highly porous network structures, displayed superior catalytic performance, excellent stability and desirable tolerance for $NaBH_4$ electrooxidation in NaOH solution. The oxidation current density of 35.4 mA cm^{-2} mg^{-1} was achieved on the Co NF@carbon sponge electrode in 1 mol L^{-1} NaOH and 0.12 mol L^{-1} $NaBH_4$ solution at −0.55 V (vs. Ag/AgCl). The promoted activity was attributed to the special 3D nano-flake structure of electrode, which guaranteed high utilization of catalysts and quick mass transport for both reactants and products in the electrochemical reactions. In a word, the neoteric Co NF@carbon sponge electrode is a promising candidate as the high-performance and low-cost anode in the application of fuel cells that use $NaBH_4$ as the fuel.

Acknowledgements

We gratefully acknowledge the financial support of this research by the National Natural Science Foundation of China (21403044), the Natural Science Foundation of Heilongjiang Province of China (LC2015004), the China Postdoctoral Science Special Foundation (2015T80329), the Heilongjiang Postdoctoral Fund (LBH-Z13059), the China Postdoctoral Science Foundation (2014M561332), the Major Project of Science and Technology of Heilongjiang Province (GA14A101) and the Project of Research and Development of Applied Technology of Harbin (2014DB4AG016).

Notes and references

1 R. Ojani, R. Valiollahi and J.B. Raoof, Au hollow nanospheres on graphene support as catalyst for sodium borohydride electrooxidation, *Appl. Surf. Sci.*, 2014, **311**, 245–251.

2 K. Ye, F. Guo, Y. Gao, D. Zhang, K. Cheng, W. Zhang, G. Wang and D. Cao, Three-dimensional carbon- and binder-free nickel nanowire arrays as a high-performance and low-cost anode for direct hydrogen peroxide fuel cell, *J. Power Sources*, 2015, **300**, 147–156.

3 K. Ye, Y. Aoki, E. Tsuji, S. Nagata and H. Habazaki, Thickness dependence of proton conductivity of anodic ZrO_2–WO_3–SiO_2 nanofilms, *J. Power Sources*, 2012, **205**, 194–200.

4 J. Ma, N.A. Choudhury and Y. Sahai, A comprehensive review of direct borohydride fuel cells, *Renew. Sust. Energ. Rev.*, 2010, **14**, 183–199.

5 K. Ye, Y. Aoki, E. Tsuji, S. Nagata and H. Habazaki, Compositional dependence of the proton conductivity of anodic ZrO_2–WO_3–SiO_2 nanofilms at intermediate temperatures, *J. Electrochem. Soc.*, 2013, **160**, F1096–F1102.

6 K. Ye, Y. Aoki, E. Tsuji, S. Nagata and H. Habazaki, Improved thermal stability of efficient proton-conducting anodic ZrO_2-WO_3 nanofilms by incorporation of silicon species, *J. Electrochem. Soc.*, 2011, **158**, C385–C390.

7 C. Celik, F.G.B. San and H.I. Sarac, Improving the direct borohydride fuel cell performance with thiourea as the additive in the sodium borohydride solution, *Int. J. Hydrogen Energy*, 2010, **35**, 8678–8682.

8 C. Celik, F.G.B. San and H.I. Sarac, Influences of sodium borohydride concentration on direct borohydride fuel cell performance, *J. Power Sources*, 2010, **195**, 2599–2603.

9 C. Celik, F.G.B. San and H.I. Sarac, Effects of operation conditions on direct borohydride fuel cell performance, *J. Power Sources*, 2008, **185**, 197–201.

10 C. Celik, F.G.B. San and H.I. Sarac, Investigation of Ni foam effect for direct borohydride fuel cell, *Fuel Cells*, 2012, **12**, 1027–1031.

11 E. Gyenge, M. Atwan and D. Northwood, Electrocatalysis of borohydride oxidation on colloidal Pt and Pt-alloys (Pt-Ir, Pt-Ni, and Pt-Au) and application for direct borohydride fuel cell anodes, *J. Electrochem. Soc.*, 2006, **153**, A150–A158.

12 D.M.F. Santos, T.F.B. Gomes, B. Šljukić, N. Sousa, C.A.C. Sequeira and F.M.L. Figueiredo, Perovskite cathodes for $NaBH_4/H_2O_2$ direct fuel cells, *Electrochim. Acta* , 2015, **178**, 163–170.

13 C. Grimmer, M. Grandi, R. Zacharias, B. Cermenek, H. Weber, C. Morais, T.W. Napporn, S. Weinberger, A. Schenk and V. Hacker, The electrooxidation of borohydride: A mechanistic study on palladium (Pd/C) applying RRDE, ^{11}B-NMR and FTIR, *Appl. Catal. B: Environ.*, 2016, **180**, 614–621.

14 B.H. Liu, Z.P. Li, K. Arai and S. Suda, Performance improvement of a micro borohydride fuel cell operating at ambient conditions, *Electrochim. Acta*, 2005, **50**, 3719–3725.

15 V. Briega-Martos, E. Herrero and J.M. Feliu, Borohydride electro-oxidation on Pt single crystal electrodes, *Electrochem. Commun.*, 2015, **51**, 144–147.

16 Z. Jusys and R.J. Behm, Borohydride electrooxidation over Pt/C, AuPt/C and Au/C catalysts: Partial reaction pathways and mixed potential formation, *Electrochem. Commun.*, 2015, **60**, 9–12.

17 B.H. Liu, J.Q. Yang and Z.P. Li, Concentration ratio of $[OH^-]/[BH_4^-]$: A controlling factor for the fuel efficiency of borohydride electro-oxidation, *Int. J. Hydrogen Energy*, 2009, **34**, 9436–9443.

18 L. Yi, W. Wei, C. Zhao, L. Tian, J. Liu and X. Wang, Enhanced activity of Au-Fe/C anodic electrocatalyst for direct borohydride-hydrogen peroxide fuel cell, *J. Power Sources*, 2015, **285**, 325–333.

19 M.G. Hosseini, M. Abdolmaleki and F. Nasirpouri, Investigation of the porous nanostructured Cu/Ni/AuNi electrode for sodium borohydride electrooxidation, *Electrochim. Acta*, 2013, **114**, 215–222.

20 L. Yi, L. Liu, X. Wang, X. Liu, W. Yi and X. Wang, Carbon supported Pt-Sn nanoparticles as anode catalyst for direct borohydride-hydrogen peroxide fuel cell: Electrocatalysis and fuel cell performance, *J. Power Sources*, 2013, **224**, 6–12.

21 L. Yi, L. Liu, X. Liu, X. Wang, W. Yi, P. He and X. Wang, Carbon-supported Pt-Co nanoparticles as anode catalyst for direct borohydride-hydrogen peroxide fuel cell: Electrocatalysis and fuel cell performance, *Int. J. Hydrogen Energy*, 2012, **37**, 12650–12658.

22 P. He, X. Wang, Y. Liu, X. Liu and L. Yi, Comparison of electrocatalytic activity of carbon-supported Au-M (M=Fe, Co, Ni, Cu and Zn) bimetallic nanoparticles for direct borohydride fuel cells, *Int. J. Hydrogen Energy*, 2012, **37**, 11984–11993.

23 L. Yi, Y. Song, X. Wang, L. Yi, J. Hu, G. Su, W. Yi and H. Yan, Carbon supported palladium hollow nanospheres as anode catalysts for direct borohydride-hydrogen peroxide fuel cells, *J. Power Sources*, 2012, **205**, 63–70.

24 J. Ma, Y. Sahai and R.G. Buchheit, Direct borohydride fuel cell using Ni-based composite anodes, *J. Power Sources*, 2010, **195**, 4709–4713.

25 D. Duan, J. Liang, H. Liu, X. You, H. Wei, G. Wei and S. Liu, The effective carbon supported core-shell structure of Ni@Au catalysts for electro-oxidation of borohydride, *Int. J. Hydrogen Energy*, 2015, **40**, 488–500.

26 M. Zhiani and I. Mohammadi, Performance study of passive and active direct borohydride fuel cell employing a commercial Pd decorated Ni-Co/C anode catalyst, *Fuel*, 2016, **166**, 517–525.

27 U.B. Demirci and P. Miele, Reaction mechanisms of the hydrolysis of sodium borohydride: A discussion focusing on cobalt-based catalysts, *C. R. Chimie*, 2014, **17**, 707–716.

28 D.M.F. Santos and C.A.C. Sequeira, Sodium borohydride as a fuel for the future, *Renew. Sust. Energ. Rev.*, 2011, **15**, 3980–4001.

29 P.I. Iotov, S.V. Kalcheva and I.A. Kanazirski, On the enhanced electrocatalytic performance of PtAu alloys in borohydride oxidation, *Electrochim. Acta*, 2013, **108**, 540–546.

30 B.H. Liu and Z.P. Li, A review: Hydrogen generation from borohydride hydrolysis reaction, *J. Power Sources*, 2009, **187**, 527–534.

31 D. Zhang, K. Ye, K. Cheng, D. Cao, J. Yin, Y. Xu and G. Wang, High electrocatalytic activity of cobalt-multiwalled carbon nanotubes-cosmetic cotton nanostructures for sodium borohydride electrooxidation, *Int. J. Hydrogen Energy*, 2014, **39**, 9651–9657.

32 D. Zhang, K. Ye, J. Yin, K. Cheng, D. Cao and G. Wang, Low-cost and binder-free, paper-based cobalt electrode for sodium borohydride electro-oxidation, *New J. Chem.*, 2014, **38**, 5376–5381.

33 D. Zhang, K. Ye, D. Cao, B. Wang, K. Cheng, Y. Li, G. Wang and Y. Xu, Co@MWNTs-Plastic: A novel electrode for $NaBH_4$ oxidation, *Electrochim. Acta*, 2015, **156**, 102–107.

34 J. Liu, H. Wang, C. Wu, Q. Zhao, X. Wang and L. Yi, Preparation and characterization of nanoporous carbon-supported platinum as anode electrocatalyst for direct borohydride fuel cell, *Int. J. Hydrogen Energy*, 2014, **39**, 6729–6736.

35 D.M.F. Santos, P.G. Saturnino, D. Macciò, A. Saccone and C.A.C. Sequeira, Platinum-rare earth intermetallic alloys as anode electrocatalysts for borohydride oxidation, *Catal. Today*, 2011, **170**, 134–140.

36 G. Wang, X. Wang, R. Miao, D. Cao and K. Sun, Effects of alkaline treatment of hydrogen storage alloy on electrocatalytic activity for $NaBH_4$ oxidation, *Int. J. Hydrogen Energy*, 2010, **35**, 1227–1231.

37 L. Wang, C. Ma and X. Mao, $LmNi_{4.78}Mn_{0.22}$ alloy modified with Si used as anodic materials in borohydride fuel cells, *J. Alloy. Compd.*, 2005, **397**, 313–316.

38 Z. Yang, L. Wang, Y. Gao, X. Mao and C. Ma, $LaNi_{4.5}Al_{0.5}$ alloy doped with Au used as anodic materials in a borohydride fuel cell, *J. Power Sources*, 2008, **184**, 260–264.

39 L. Wang, C. Ma, X. Mao, Y. Sun and S. Suda, AB_5-type hydrogen storage alloy modified with Ti/Zr used as anodic materials in borohydride fuel cell, *J. Mater. Sci. Technol.*, 2005, **21**, 831–835.

40 D. Zhang, G. Wang, K. Cheng, J. Huang, P. Yan and D. Cao, Enhancement of electrocatalytic performance of hydrogen storage alloys by multi-walled carbon nanotubes for sodium borohydride oxidation, *J. Power Sources*, 2014, **245**, 482–486.

41 D. Duan, Y. Zhao, S. Liu and A. Wu, Electrochemical oxidation of borohydride on Cu electrode, *Adv. Mater. Res.*, 2012, **347–353**, 3264–3267.

42 K. Ye, D. Zhang, F. Guo, K. Cheng, G. Wang and D. Cao, Highly porous nickel@carbon sponge as a novel type of three-dimensional anode with low cost for high catalytic performance of urea electro-oxidation in alkaline medium, *J. Power Sources*, 2015, **283**, 408–415.

43 K. Ye, D. Zhang, X. Wang, K. Cheng and D. Cao, A novel three-dimensional gold catalyst prepared by simple pulse electrodeposition and its high electrochemical performance for hydrogen peroxide reduction, *RSC Adv.*, 2015, **5**, 3239–3247.
44 X. Wang, K. Ye, Y. Gao, H. Zhang, K. Cheng, X. Xiao, G. Wang and D. Cao, Preparation of porous palladium nanowire arrays and their catalytic performance for hydrogen peroxide electroreduction in acid medium, *J. Power Sources*, 2016, **303**, 278–286.
45 F. Guo, K. Ye, M. Du, K. Cheng, Y. Gao, G. Wang and D. Cao, Nickel nanowire arrays electrode as an efficient catalyst for urea peroxide electro-oxidation in alkaline media, *Electrochim. Acta*, 2016, **190**, 150–158.
46 P. Xu, K. Ye, D. Cao, J. Huang, T. Liu, K. Cheng, J. Yin and G. Wang, Facile synthesis of cobalt manganese oxides nanowires on nickel foam with superior electrochemical performance, *J. Power Sources*, 2014, **268**, 204–211.
47 K. Ye, D. Zhang, H. Zhang, K. Cheng, G. Wang, D. Cao, Platinum-modified cobalt nanosheets supported on three-dimensional carbon sponge as a high-performance catalyst for hydrogen peroxide electroreduction, *Electrochim. Acta*, 2015, **178**, 270–279.
48 F. Guo, K. Ye, X. Huang, Y. Gao, K. Cheng, G. Wang and D. Cao, Palladium dispersed in three-dimensional polyaniline networks as the catalyst for hydrogen peroxide electro-reduction in an acidic medium, *RSC Adv.*, 2015, **5**, 94008–94015.
49 D. Zhang, D. Cao, K. Ye, J. Yin, K. Cheng and G. Wang, Cobalt nano-sheet supported on graphite modified paper as a binder free electrode for peroxide electrooxidation, *Electrochim. Acta*, 2014, **139**, 250–255.
50 X. Cheng, K. Ye, D. Zhang, K. Cheng, Y. Li, B. Wang, G. Wang and D. Cao, Methanol electrooxidation on flexible multi-walled carbon nanotube-modified sponge-based nickel electrode, *J. Solid State Electrochem.*, 2015, **19**, 3027–3034.
51 W. Chen, R.B. Rakhi, L. Hu, X. Xie, Y. Cui and H.N. Alshareef, High-performance nanostructured supercapacitors on a sponge, *Nano Lett.*, 2011, **11**, 5165–5172.
52 C. Liu, T. Ko, W. Kuo, H. Chou, H. Chang and Y. Liao, Effect of carbon fiber cloth with different structure on the performance of low temperature proton exchange membrane fuel cells, *J. Power Sources*, 2009, **186**, 450–454.
53 H.B. Noh, K.S. Lee, P. Chandra, M.S. Won and Y.B. Shim, Application of a Cu–Co alloy dendrite on glucose and hydrogen peroxide sensors, *Electrochim. Acta*, 2012, 61, 36–43.
54 D. Zhang, K. Cheng, N. Shi, F. Guo, G. Wang and D. Cao, Nickel particles supported on multi-walled carbon nanotubes modified sponge for sodium borohydride electrooxidation, *Electrochem. Commun.*, 2013, **35**, 128–130.
55 R. Liu, X. Jiang, F. Guo, N. Shi, J. Yin, G. Wang and D. Cao, Carbon fiber cloth supported micro- and nano-structured Co as the electrode for hydrazine oxidation in alkaline media, *Electrochim. Acta*, 2013, **94**, 214–218.